Mathematical Medicine and Biology (2016) **33**, 87–106
doi:10.1093/imammb/dqv005
Advance Access publication on March 19, 2015

Conduction of feedback-mediated signal in a computational model of coupled nephrons

Ioannis Sgouralis*
National Institute for Mathematical and Biological Synthesis, University of Tennessee, Knoxville, TN, USA
*Corresponding author: sgouralis@nimbios.org

and

Anita T. Layton
Department of Mathematics, Duke University, Durham, NC, USA

[Received on 26 October 2014; revised on 14 January 2015; accepted on 17 February 2015]

The nephron in the kidney regulates its fluid flow by several autoregulatory mechanisms. Two primary mechanisms are the myogenic response and the tubuloglomerular feedback (TGF). The myogenic response is a property of the pre-glomerular vasculature in which a rise in intravascular pressure elicits vasoconstriction that generates a compensatory increase in vascular resistance. TGF is a negative feedback response that balances glomerular filtration with tubular reabsorptive capacity. While each nephron has its own autoregulatory response, the responses of the kidney's many nephrons do not act autonomously but are instead coupled through the pre-glomerular vasculature. To better understand the conduction of these signals along the pre-glomerular arterioles and the impacts of internephron coupling on nephron flow dynamics, we developed a mathematical model of renal haemodynamics of two neighbouring nephrons that are coupled in that their afferent arterioles arise from a common cortical radial artery. Simulations were conducted to estimate internephron coupling strength, determine its dependence on vascular properties and to investigate the effect of coupling on TGF-mediated flow oscillations. Simulation results suggest that reduced gap-junctional conductances may yield stronger internephron TGF coupling and highly irregular TGF-mediated oscillations in nephron dynamics, both of which experimentally have been associated with hypertensive rats.

Keywords: haemodynamics; tubuloglomerular feedback; myogenic response; afferent arteriole; nonlinear dynamics.

1. Introduction

The fundamental role of the kidney is to remove metabolic waste from the body while maintaining a balance of volume, electrolytes and acid–base (Eaton & Pooler, 2004). That balance is achieved, in large part, by processes that take place in the individual functional unit of the kidney, the nephron. Each nephron consists of a filtering component, termed glomerulus and a renal tubule. A single afferent arteriole delivers blood to the glomerulus. About one-fifth of the blood plasma is filtered through the glomerular capillaries to become filtrate that enters the renal tubule. The epithelial transport processes along the tubule continuously modify the composition of the filtrate, such that eventually most of the filtered water and electrolytes are reabsorbed and returned to general circulation. The number of nephrons in a kidney depends on body size. A rat kidney is composed of ∼30,000–40,000 nephrons (Han *et al.*, 1992); a human kidney contains up to a million nephrons (Nyengaard & Bendtsen, 1992).

Epithelial transport and tubular luminal fluid composition are influenced substantially by fluid flow, which is in turn determined, in part, by the glomerular filtration rate (GFR). Thus, regulation of the GFR is essential for proper kidney function. One regulatory mechanism is the myogenic response, in which the afferent arteriolar muscles respond to perturbations in intraluminal pressure or stretch with active force development, thereby enabling the arteriole to constrict, reducing glomerular blood delivery and the GFR (Holstein-Rathlou & Marsh, 1994; Just, 2007).

Another contributing mechanism is a negative feedback system, termed tubuloglomerular feedback (TGF), by which the nephron controls incoming blood flow and the GFR by responding to variations in the ionic composition of loop of Henle outflow (Holstein-Rathlou & Marsh, 1994; Just, 2007). A specialized cluster of cells, termed macula densa (MD), senses the Cl^- concentration in the tubular fluid flowing past that area and generates a signal that adjusts the GFR by changing the afferent arteriole smooth muscle tone. Taken in isolation, a higher GFR results in a higher tubular fluid Cl^- concentration. The MD cells respond by inducing a constriction of smooth muscles in the afferent arteriole to increase vascular resistance, thereby lowering blood flow and thus the GFR. Conversely, the TGF system responds to a low $[Cl^-]$ by dilating the afferent arteriole to increase blood flow and the GFR.

In a series of studies, we developed a detailed mathematical model of renal haemodynamics (Chen *et al.*, 2011; Sgouralis & Layton, 2012, 2014a,b). The model by Sgouralis & Layton (2014b) represents an afferent arteriole, glomerular filtration, Cl^- transport along the proximal segments of a short-loop nephron and TGF. The model afferent arteriole is myogenically active and represents smooth muscle membrane potential and gap-junctional coupling. The activity of non-selective cation channels is assumed to be shifted by changes in intravascular pressure, and thus the smooth muscle membrane depolarizes with increasing intravascular pressure, such that elevation in pressure induces vasoconstriction which increases resistance to blood flow. We used that model to assess the individual contributions of TGF and myogenic response to GFR regulation in the rat kidney.

The model by Sgouralis & Layton (2014b) represents an isolated nephron with the associated vasculature, whereas, as noted above, ∼30,000–40,000 nephrons are packed inside a rat kidney. Indeed, experimental observation in rats has indicated that individual nephrons do not operate independently but interact constantly with the neighbouring nephrons. This coupling effect is mediated by the propagation of TGF-induced electrotonic signals along the pre-glomerular vasculature (Holstein-Rathlou, 1987; Källskog & Marsh, 1990; Yip *et al.*, 1992). For instance, if two afferent arterioles associated with two nephrons are fed by a common cortical radial artery, then the contraction of one nephron's afferent arteriole likely causes the other afferent arteriole to contract too.

Results of previous modelling studies have suggested that internephron coupling may have a significant impact on the TGF-mediated dynamics of nephron flow and other variables (Pitman *et al.*, 2004; Layton *et al.*, 2006, 2009, 2011). While those studies represent Cl^- transport along the thick ascending limb in detail, the afferent arteriole is not represented explicitly, and the conduction of the TGF signal via the coupled afferent arterioles is represented only phenomenologically. A goal of this study is to better characterize the coupling, in the context of TGF, between two neighbouring nephrons.

To that end, we extend the renal haemodynamics model of Sgouralis & Layton (2014b) to a pair of nephrons whose afferent arterioles arise from the same cortical radial artery. We use the coupled nephron model to study the conduction of TGF signals along the afferent arterioles, and we investigate how TGF-mediated tubular flow dynamics is impacted by internephron coupling.

2. Mathematical model

A schematic diagram of the coupled-nephron model is given in Fig. 1. The model represents a connecting artery that branches off the cortical radial artery and divides into a pair of afferent arterioles. Model

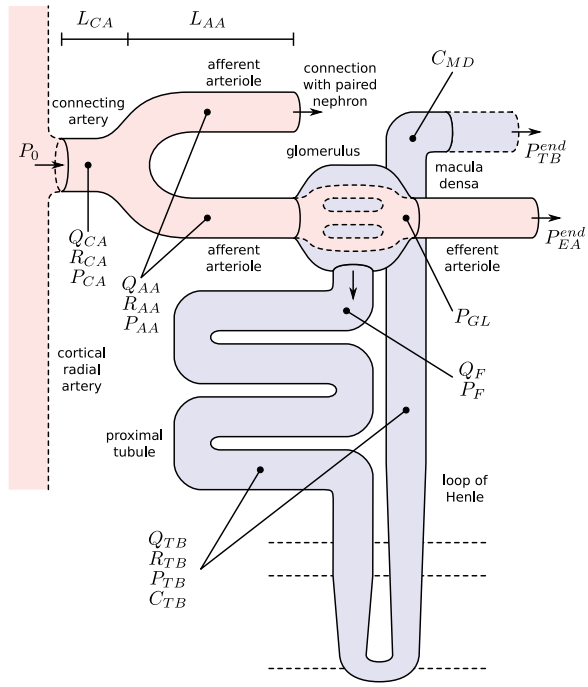

FIG. 1. Schematic representation of the coupled nephrons model. Both afferent arterioles are shown, while glomerulus and tubular segments are shown only for one of the paired nephrons. *Q*, fluid flow; *R*, tubular or vascular radius; *P*, fluid pressure. Subscripts 'CA' denote connecting artery; 'AA', afferent arteriole; 'EA', efferent arteriole; 'GL', glomerulus; 'F', proximal tubule entrance; 'TB', renal tubule. C_{MD}, tubular fluid [Cl^-] at the macula densa.

geometry is based on anatomic findings by Casellas *et al.* (1994). Each afferent arteriole is connected to a model glomerulus and a short-loop nephron segment. The representation of model components is based on our previous work (Sgouralis & Layton, 2014b). Below we describe the vascular and tubular components. The two nephrons are indexed by j, where $j = 1$ or 2.

2.1 *Vascular submodel*

The jth model afferent arteriole consists of a series of smooth muscle cell models (Sgouralis & Layton, 2012, 2014a,b), electrically coupled via gap-junctions and via an endothelial layer. The cellular ionic transport dynamics of each smooth muscle cell, influenced by the autoregulatory mechanisms, determine the local vascular tone. The resulting vascular resistance is the main determinant of blood flow and single-nephron glomerular filtration rate (SNGFR).

Each smooth muscle cell model incorporates cell membrane potential, transmembrane ionic transport, cytosolic Ca^{2+} regulation and muscle contraction. The interactions between the Ca^{2+} and K^+ fluxes, which are mediated by voltage-gated and voltage–calcium-gated channels, respectively, give rise to the development of spontaneous oscillations in membrane potential. This in turn results in oscillations in cytoplasmic Ca^{2+} concentration and muscle tone. Details of the ionic transport, Ca^{2+} dynamics, crossbridges phosphorylation and muscle mechanics can be found in Chen *et al.* (2011), Sgouralis & Layton (2012) and Sgouralis & Layton (2014a,b). Below we summarize key model components.

2.1.1 *Smooth muscle cell membrane potential.* The smooth muscle cells that form the jth afferent arteriole are indexed by i, where $i = 1$ and $i = N^j_{\mathrm{AA}}$ denote the cells closest to the connecting artery ($z = 0$) and glomerulus ($z = L^j_{\mathrm{AA}}$), respectively. The associated endothelial compartments are indexed analogously. Throughout this study, let subscripts m and e denote the muscle and endothelial cells, respectively. The rate of change of the membrane potentials of the ith smooth muscle and endothelial cells, denoted by $v^{i,j}_m$ and $v^{i,j}_e$, respectively, are given by

$$C^j_m \frac{\mathrm{d}v^{i,j}_m}{\mathrm{d}t} = -I^{i,j}_{\mathrm{L}} - I^{i,j}_{\mathrm{K}} - I^{i,j}_{\mathrm{Ca}} + I^{i,j}_{mm} + I^{i,j}_{me} + I^{i,j}_{\mathrm{MR}} + I^{i,j}_{\mathrm{TGF}}, \tag{2.1}$$

$$C^j_e \frac{\mathrm{d}v^{i,j}_e}{\mathrm{d}t} = -I^{i,j}_{me} + I^{i,j}_{ee}, \tag{2.2}$$

where C^j_m and C^j_e denote cellular capacitances, assumed spatially independent but may differ between arterioles. By $I^{i,j}_{\mathrm{L}}$ $I^{i,j}_{\mathrm{K}}$, and $I^{i,j}_{\mathrm{Ca}}$ we denote transmembrane leak current, potassium current and calcium current, respectively; $I^{i,j}_{mm}$, $I^{i,j}_{me}$ and $I^{i,j}_{ee}$ are gap-junctional currents; and $I^{i,j}_{\mathrm{MR}}$ and $I^{i,j}_{\mathrm{TGF}}$ are myogenic- and TGF-induced currents.

The transmembrane currents are given by

$$I^{i,j}_{\mathrm{L}} = g^j_{\mathrm{L}}(v^{i,j}_m - v^j_{\mathrm{L}}), \tag{2.3}$$

$$I^{i,j}_{\mathrm{K}} = g^j_{\mathrm{K}} n^{i,j}(v^{i,j}_m - v^j_{\mathrm{K}}), \tag{2.4}$$

$$I^{i,j}_{\mathrm{Ca}} = g^j_{\mathrm{Ca}} m^{i,j}(v^{i,j}_m - v^j_{\mathrm{Ca}}), \tag{2.5}$$

where $n^{i,j}$ and $m^{i,j}$ denote the fraction of open K^+ and Ca^{2+} channels, respectively. The model assumes that $n^{i,j}$ depends on $v^{i,j}_m$ as well as on cytosolic $[Ca^{2+}]$, whereas $m^{i,j}$ depends only on $v^{i,j}_m$. For details see Chen *et al.* (2011) and Sgouralis & Layton (2014a). The remaining currents, $I^{i,j}_{\mathrm{MR}}$ and $I^{i,j}_{\mathrm{TGF}}$, arise from the operation of the myogenic response and TGF (see below).

Neighbouring afferent arteriole smooth muscle cells communicate via homocellular and heterocellular gap-junctions (Brink, 1998; Wagner, 2008). We consider gap-junctional currents passing between smooth muscles, denoted by $I^{i,j}_{mm}$, between smooth muscles and the endothelium, denoted by $I^{i,j}_{me}$, and between endothelial cells, denoted by $I^{i,j}_{ee}$. (Recall subscripts m and e indicate smooth muscle and endothelial cells, respectively.) The smooth muscle–endothelium gap-junction current in Equation (2.2) is given by Ohm's law

$$I^{i,j}_{me} = g^j_{me}(v^{i,j}_e - v^{i,j}_m). \tag{2.6}$$

Similarly, away from the boundaries, i.e. for $i = 2, \ldots N^j_{\mathrm{AA}} - 1$, the gap-junction currents $I^{i,j}_{mm}$ and $I^{i,j}_{ee}$ are, respectively, given by

$$I^{i,j}_{mm} = g^j_{mm}(v^{i-1,j}_m - 2v^{i,j}_m + v^{i+1,j}_m), \tag{2.7}$$

$$I^{i,j}_{ee} = g^j_{ee}(v^{i-1,j}_e - 2v^{i,j}_e + v^{i+1,j}_e). \tag{2.8}$$

To implement electrotonic coupling of the two nephrons, we assume that, at the junction with the connecting artery ($i = 1$), the two afferent arterioles are attached to a common node with potentials v^*_m and v^*_e, with gap-junctional conductances denoted by g^*_{mc} and g^*_{ec}, respectively; see Fig. 2. (The subscript

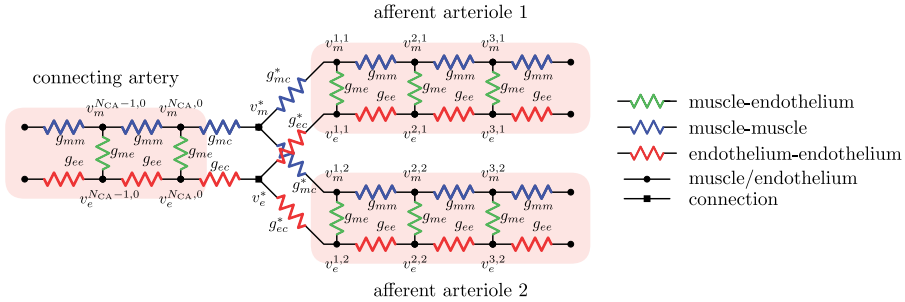

FIG. 2. Equivalent circuit of intercellular coupling near the vascular junction. For simplicity, only gap-junctional currents are shown. Both homocellular and heterocellular interfaces are represented.

c indicates 'connection'.) This yields the boundary conditions

$$I^{1,j}_{mm} = g^{j}_{mm}(v^{2,j}_{m} - v^{1,j}_{m}) + g^{*}_{mc}(v^{*}_{m} - v^{1,j}_{m}), \tag{2.9}$$

$$I^{1,j}_{ee} = g^{j}_{ee}(v^{2,j}_{e} - v^{1,j}_{e}) + g^{*}_{ec}(v^{*}_{e} - v^{1,j}_{e}). \tag{2.10}$$

In the base case, $g^{*}_{mc} = g_{mm}$ and $g^{*}_{ec} = g_{ee}$.

The boundary condition at $i = N^{j}_{\mathrm{AA}}$, which represents current leakage out of the vessel, can be found in Sgouralis & Layton (2012, 2014a).

2.1.2 *Myogenic response.* We assume that the activity of non-selective cation channels responds to changes in intravascular pressure, such that elevations in intravascular pressure depolarize the smooth muscle membrane and *vice versa*. To induce pressure-dependent changes in membrane potential, we apply a current $I^{i,j}_{\mathrm{MR}}$ in Equation (2.1), which is described by

$$\frac{\mathrm{d}}{\mathrm{d}t} I^{i,j}_{\mathrm{MR}} = \begin{cases} -k^{j}_{\mathrm{inc}}(I^{i,j}_{\mathrm{MR}}(t) - \bar{I}^{i,j}_{\mathrm{MR}}(P^{i,j}_{\mathrm{AA}}(t))) & \text{if } \dfrac{\mathrm{d}}{\mathrm{d}t} P^{i,j}_{\mathrm{AA}}(t - \tau^{j}_{m}) \geqslant 0, \\ -k^{j}_{\mathrm{dec}}(I^{i,j}_{\mathrm{MR}}(t) - \bar{I}^{i,j}_{\mathrm{MR}}(P^{i,j}_{\mathrm{AA}}(t))) & \text{if } \dfrac{\mathrm{d}}{\mathrm{d}t} P^{i,j}_{\mathrm{AA}}(t - \tau^{j}_{m}) < 0, \end{cases} \tag{2.11}$$

where $P^{i,j}_{\mathrm{AA}}$ denotes the intravascular pressure. Equation (2.11) describes a rate-dependent myogenic response, in which $\mathrm{d}I^{i,j}_{\mathrm{MR}}/\mathrm{d}t$ at time t depends on the *direction* that $P^{i,j}_{\mathrm{AA}}$ is changing at an earlier time $t - \tau^{j}_{m}$, as indicated by experimental observations (Loutzenhiser *et al.*, 2002, 2004). The asymmetric rate constants k^{j}_{inc} and k^{j}_{dec} are set to 0.55 and 0.13 s^{-1} for both nephrons, consistent with experimental measurements (Loutzenhiser & Loutzenhiser, 2000). Similarly, the response delay τ^{j}_{m} of both nephrons is set to 0.3 s for pressure increases and to 1 s for pressure decreases (Loutzenhiser *et al.*, 2002, 2004).

To represent a depolarizing current at elevated blood pressure, we assume that the target current $\bar{I}^{ij,}_{\mathrm{MR}}$ is an increasing function of luminal pressure having the saturable form

$$\bar{I}^{i,j}_{\mathrm{MR}}(P^{i,j}_{\mathrm{AA}}) = I^{j}_{\mathrm{MR,min}} + \frac{I^{j}_{\mathrm{MR,max}} - I^{j}_{\mathrm{MR,min}}}{1 - (I^{j}_{\mathrm{MR,max}}/I^{j}_{\mathrm{MR,min}}) \exp(-s^{j}_{\mathrm{MR}}(P^{i,j}_{\mathrm{AA}}(t - \tau^{j}_{m}) - \bar{P}^{i,j}_{\mathrm{AA}}))}. \tag{2.12}$$

The reference pressure $\bar{P}^{i,j}_{\mathrm{AA}}$ is chosen such that at baseline perfusion pressure $\bar{I}^{i,j}_{\mathrm{MR}}$ is zero.

2.1.3 *Tubuloglomerular feedback.* The TGF current is applied to the smooth muscles spanning only the distal 60 μm of the afferent arterioles (Christensen & Bohle, 1978). The current $I^{i,j}_{\mathrm{TGF}}$ is assumed to exhibit a sigmoidal dependence on intratubular macula densa [Cl^-] (denoted by C^j_{MD}),

$$I^{i,j}_{\mathrm{TGF}}(C^j_{\mathrm{MD}}) = I^j_{\mathrm{TGF,min}} + \frac{I^j_{\mathrm{TGF,max}} - I^j_{\mathrm{TGF,min}}}{1 - (I^j_{\mathrm{TGF,max}}/I^j_{\mathrm{TGF,min}})\exp(-s^j_{\mathrm{TGF}}(C^j_{\mathrm{MD}} - \bar{C}^j_{\mathrm{MD}}))}, \tag{2.13}$$

where $\bar{C}^j_{\mathrm{MD}}$ denotes the operating macula densa [Cl^-], set to 32 mM for both nephrons (Layton *et al.*, 1991). The parameters $I^j_{\mathrm{TGF,max}}$, $I^j_{\mathrm{TGF,min}}$ and s^j_{TGF} determine the dynamic range and open-loop gain of TGF; for details see Sgouralis & Layton (2014b).

2.1.4 *Connecting artery.* Representation of the connecting artery follows that of the afferent arteriole. Smooth muscle membrane and endothelium potentials are given by

$$C^0_m \frac{\mathrm{d}v^{i,0}_m}{\mathrm{d}t} = -I^{i,0}_{\mathrm{L}} - I^{i,0}_{\mathrm{K}} - I^{i,0}_{\mathrm{Ca}} + I^{i,0}_{mm} + I^{i,0}_{me} + I^{i,0}_{\mathrm{MR}}, \tag{2.14}$$

$$C^0_e \frac{\mathrm{d}v^{i,0}_e}{\mathrm{d}t} = -I^{i,0}_{me} + I^{i,0}_{ee}, \tag{2.15}$$

where $j = 0$ denotes the connecting artery. At the junction with the arterioles ($i = N_{\mathrm{CA}}$), muscle and endothelial potentials are connected to v^*_m and v^*_e with conductances $g_{mc} = 2g_{mm}$ and $g_{ec} = 2g_{ee}$, respectively; see Fig. 2. The values of v^*_m and v^*_e are determined by conservation of current

$$g_{mc}(v^*_m - v^{N_{\mathrm{CA}},0}_m) = g^*_{mc}(v^{1,1}_m - v^*_m) + g^*_{mc}(v^{1,2}_m - v^*_m), \tag{2.16}$$

$$g_{ec}(v^*_e - v^{N_{\mathrm{CA}},0}_e) = g^*_{ec}(v^{1,1}_e - v^*_e) + g^*_{ec}(v^{1,2}_e - v^*_e). \tag{2.17}$$

2.1.5 *Blood flow.* Blood enters the cortical radial artery at the renal perfusion pressure P_{RA}, which is assumed known *a priori* and is given by

$$P_{\mathrm{RA}} = P_{\mathrm{m}} + P_{\mathrm{p}} \sin(2\pi f t), \tag{2.18}$$

where $P_{\mathrm{m}} = 100$ mmHg is the mean arterial pressure, $P_{\mathrm{p}} = 20$ mmHg is the pulse amplitude and $f = 6$ Hz is the heart rate typical of a rat. The pulse amplitude P_{p} is chosen to be smaller than the heart beat amplitude to reflect the damping that occurs upstream of the connecting artery and the afferent arterioles.

We assume simple Poiseuille flow so that blood flow can be computed from the pressure drop along the vessel and the vascular resistance. Let Q_{CA} and Q^j_{AA} denote blood flow along the connecting artery and the jth afferent arteriole, respectively. Then

$$Q^j_{\mathrm{AA}} = \frac{P^j_{\mathrm{AA}}(t,0) - P^j_{\mathrm{AA}}(t, L^j_{\mathrm{AA}})}{\Omega^j_{\mathrm{AA}}}, \tag{2.19}$$

where $P^j_{\mathrm{AA}}(t,z)$ is the pressure profile along the jth afferent arteriole. Conservation of mass implies

$$Q_{\mathrm{CA}} = Q^1_{\mathrm{AA}} + Q^2_{\mathrm{AA}}. \tag{2.20}$$

The overall resistance of each afferent arteriole is computed from the radius profile

$$\Omega^j_{\mathrm{AA}} = \frac{8\mu}{\pi}\int_0^{L^j_{\mathrm{AA}}} \frac{\mathrm{d}z}{R^j_{\mathrm{AA}}(t,z)^4}, \tag{2.21}$$

where R^j_{AA} denotes arteriolar radius and μ denotes the apparent blood viscosity.

We assume that each model afferent arteriole is connected in series to a post-glomerular resistor Ω^j_{EA} at the end of which pressure is $P_{\mathrm{EA,end}} = 0$ mmHg. Post-glomerular blood flow is given by the difference between arteriolar flow Q^j_{AA} and SNGFR (denoted by Q^j_{F}), and is related to pressure drop and vascular resistance according to

$$Q^j_{\mathrm{AA}} - Q^j_{\mathrm{F}} = \frac{P^j_{\mathrm{GL}} - P_{\mathrm{EA,end}}}{\Omega^j_{\mathrm{EA}}}, \tag{2.22}$$

where P^j_{GL} is the blood pressure at the end of the glomerular capillary. The relation between P^j_{AA} and P^j_{GL} can be found in Sgouralis & Layton (2014b). The values of Ω^j_{EA} are chosen such that, in the base case, they account for 47% of the pressure drop between P_{m} and $P_{\mathrm{EA,end}}$.

The pressure gradient along the vascular lumens is given by the Poiseuille equation

$$\frac{\mathrm{d}P_{\mathrm{CA}}(t,z)}{\mathrm{d}z} = -\frac{8\mu}{\pi(R_{\mathrm{CA}}(t,z))^4} Q_{\mathrm{CA}}(t), \quad 0 < z < L_{\mathrm{CA}}, \tag{2.23}$$

$$\frac{\mathrm{d}P^j_{\mathrm{AA}}(t,z)}{\mathrm{d}z} = -\frac{8\mu}{\pi(R^j_{\mathrm{AA}}(t,z))^4} Q^j_{\mathrm{AA}}(t), \quad 0 < z < L_{\mathrm{AA}}, \tag{2.24}$$

where $P_{\mathrm{CA}}(t,z)$ is the pressure along the connecting artery. Before entering the connecting artery, blood is assumed passing through a fixed resistor Ω_{RA}, thus pressure at the connecting artery's inlet is given by $P_0 = P_{\mathrm{RA}} - Q_{\mathrm{CA}}\Omega_{\mathrm{RA}}$. The value of Ω_{RA} is chosen such that at baseline it accounts for a pressure drop of 5 mmHg, (Sgouralis & Layton, 2014b). At the vascular junction, continuity of blood pressure implies $P_{\mathrm{CA}}(t, L_{\mathrm{CA}}) = P^j_{\mathrm{AA}}(t,0)$ for $j = 1$ and 2.

To represent the differences in the geometric dimensions between the afferent arterioles and the connecting arteries, as seen in Casellas *et al.* (1994) and Wagner *et al.* (1997), the baseline vascular tone of the smooth muscles forming the connecting artery is adjusted to yield a baseline luminal radius that is 20% larger than that of the arterioles.

2.2 *Tubule submodel*

The tubule model represents a proximal tubule followed by a short-loop of Henle, extending from $x = 0$ (connection with the glomerulus) to $x = L^j_{\mathrm{TB}}$ (site of the macula densa). The model predicts intratubular pressure (P^j_{TB}), water flow rate (Q^j_{TB}) and Cl^- concentration (C^j_{TB}). Tubular walls are assumed to be

compliant, with a radius that depends passively on the transmural pressure gradient

$$R^j_{\mathrm{TB}} = \alpha^j_{\mathrm{TB}}(P^j_{\mathrm{TB}} - P_{\mathrm{ext}}) + \beta^j_{\mathrm{TB}}, \tag{2.25}$$

where α^j_{TB} characterizes tubular compliance and β^j_{TB} is the unpressurized radius.

2.2.1 *Water transport.* Tubular water flow is assumed to be pressure driven. The proximal tubule and the initial segment of the descending limb of Henle's loop are water permeable. Taking the transmural water flux Φ^j_{TB} into account, pressure and flow rate along the model nephron are, respectively, given by

$$\frac{\partial P^j_{\mathrm{TB}}(t,x)}{\partial x} = -\frac{8\mu_{\mathrm{TB}}}{\pi (R^j_{\mathrm{TB}}(t,x))^4} Q^j_{\mathrm{TB}}(t,x), \tag{2.26}$$

$$\frac{\partial Q^j_{\mathrm{TB}}(t,x)}{\partial x} = -2\pi R^j_{\mathrm{TB}}(t,x)\frac{\partial R^j_{\mathrm{TB}}(t,x)}{\partial t} - \Phi^j_{\mathrm{TB}}(t,x). \tag{2.27}$$

At its outlet (site of the macula densa), the model tubule is connected to a resistance Ω^j_{DT}, at the end of which pressure is assumed to be fixed at $P_{\mathrm{DT,end}} = 2$ mmHg. Thus, tubular outlet pressure and flow are related by

$$P^j_{\mathrm{TB}}(t, L_{\mathrm{TB}}) = P_{\mathrm{DT,end}} + Q^j_{\mathrm{TB}}(t, L^j_{\mathrm{TB}})\Omega^j_{\mathrm{DT}}. \tag{2.28}$$

For details see Sgouralis & Layton (2014b).

Transmural water flux depends on the SNGFR:

$$\Phi^j_{\mathrm{TB}} = S_{\mathrm{GTB}}(Q^j_{\mathrm{F}})\Phi^j_{\mathrm{TB,base}}, \tag{2.29}$$

where $\Phi^j_{\mathrm{TB,base}}$ is the baseline water flux profile. The factor S_{GTB} is a dimensionless scaling that models glomerulotubular balance (Thomson *et al.*, 2001; Thomson & Blantz, 2008), which is given by

$$S_{\mathrm{GTB}}(Q^j_{\mathrm{F}}) = \frac{1}{1 + 0.7(\bar{Q}^j_{\mathrm{F}}/Q^j_{\mathrm{F}} - 1)}, \tag{2.30}$$

where $\bar{Q}^j_{\mathrm{F}}$ is the operating point, set to 30 nl/min for both nephrons.

2.2.2 *Chloride transport.* Chloride concentration along the tubule is given by conservation of mass

$$\frac{\partial}{\partial t}(\pi (R^j_{\mathrm{TB}})^2 C^j_{\mathrm{TB}}) = -\frac{\partial}{\partial x}(Q^j_{\mathrm{TB}} C^j_{\mathrm{TB}}) - 2\pi R^j_{\mathrm{TB,ss}}\left(\frac{V^j_{\max} C^j_{\mathrm{TB}}}{K^j_{\mathrm{M}} + C^j_{\mathrm{TB}}} + \kappa^j_{\mathrm{TB}}(C^j_{\mathrm{TB}} - C_{\mathrm{TB,ext}})\right), \tag{2.31}$$

where $R^j_{\mathrm{TB,ss}}$ is the steady-state tubular radius. Interstitial Cl^- concentration, denoted by $C_{\mathrm{TB,ext}}$, is set to 115 mM in the cortex and increases to 275 mM at the outer–inner medullary boundary (Layton *et al.*, 1991). The first term in the last pair of parentheses corresponds to active solute transport characterized by Michaelis–Menten-like kinetics, and the second term represents transepithelial diffusion with transmural permeability κ^j_{TB}. Strictly speaking, Na^+ ion is actively transported via the Na^+/K^+-ATP pump,

with Cl^- ion transported passively through the basolateral membrane. On the apical side, the NKCC2 transporter binds one Na^+ ion for each K^+ or NH_4^+ ion plus two Cl^- ions. Thus, the Michaelis–Menten term in Equation (2.31) is an approximation and appears to be sufficient. At the entrance of the proximal tubule ($x = 0$), tubular fluid [Cl^-] is set to 115 mM.

The proximal tubule exhibits glomerulotubular balance, whereby NaCl and water reabsorption along the proximal tubular varies *in tandem*. To represent glomerulotubular balance, we assume that, along the proximal tubule, maximum active Cl^- transport $V^j_{\max}$ exhibits an analogous dependence upon the SNGFR as the transmural water flux Φ^j_{TB}. That dependence is given by

$$V^j_{\max} = (1 + 0.65(S_{\mathrm{GTB}}(Q^j_{\mathrm{F}}) - 1))V^j_{\max,\mathrm{base}}, \tag{2.32}$$

where $V^j_{\max,\mathrm{base}}$ is the baseline maximum transport rate along the proximal tubule. Note that the above relation applies only along the proximal tubule, not the downstream segments.

2.3 *Model parameters*

The model involves a large number of parameters, which have been adopted from Sgouralis & Layton (2014b) unless specified otherwise. A list of selected key parameter values can be found in Table 1.

3. Results

3.1 *Effect of coupling on TGF-mediated dynamics*

We first consider two isolated nephrons. The goal is to understand the behaviours of blood flow and solute transport in the absence of internephron coupling, and how those behaviours are affected by TGF. Similar to previous modelling studies, the afferent arterioles are assumed to be 303 μm long (Sgouralis & Layton, 2012, 2014a,b). The connecting artery is not represented; instead, perfusion pressure P_{RA} is applied at the entrance of separate pre-arteriolar resistors Ω^1_{RA} and Ω^2_{RA}, with each one having half the baseline value of Ω_{RA}. With this configuration, the nephrons are fed by non-overlapping vasculatures, and thus each one operates independently of the other.

In nephron 1, the TGF parameter s^1_{TGF} is set to 0. This corresponds to an open-loop gain of 0, and thus complete absence of TGF. SNGFR and macula densa luminal [Cl^-] time courses, shown in Fig. 3(A1 and A2) (blue line), exhibit limit-cycle oscillations at a frequency of ∼170 mHz. Those oscillations arise from the spontaneous vasomotion of the afferent arteriole, which, in turn, results from the interactions between cellular ionic fluxes and membrane potential (for a detailed explanation of the origin of the spontaneous vasomotion, see Chen *et al.*, 2011). Spontaneous vasomotion yields oscillations in arteriolar resistance, and thus the SNGFR.

In nephron 2, s^2_{TGF} is set to 0.16 mM^{-1}, which gives an open-loop gain of 3.1. At this gain, TGF-mediated oscillations in blood flow and related variables emerge, at a frequency of ∼28 mHz; see Fig. 3(A1 and A2) (red line).

Another frequency signature (6 Hz) in the blood flow arises from the heart beat (Equation (2.18)). Those oscillations are significantly attenuated by the glomerular filtration process, and then further damped by the compliance of the renal tubule. As a result, oscillations at heart rate are distinguishable only at the SNGFR (Fig. 3A1) and entirely removed from the time courses at the site of the macula densa (Fig. 3A2).

In the next set of simulations, the two nephrons are connected to a common connecting artery, as shown in Fig. 1. The SNGFR and the macula densa [Cl^-] of each nephron are shown in Fig. 3(B1 and

TABLE 1 *Baseline parameter values. Superscripts* 0, 1, 2 *refer to connecting artery, afferent arteriole* 1 *and afferent arteriole* 2*, respectively. References*: [0]*present study*, [1]*Casellas et al. (1994)*, [2]*Chilton et al. (2008)*, [3]*Sgouralis & Layton (2014b)*, [4]*Sgouralis & Layton (2012)*, [5]*Sgouralis & Layton (2014a)*, [6]*Chen et al. (2011)*

Description	Parameter	Value	Units	j
Afferent arteriole size[0]	N_{AA}^{j}	81	—	1, 2
Connecting artery size[0]	N_{CA}	20	—	—
Afferent arteriole length[0]	L_{AA}^{j}	243	μm	1, 2
Connecting artery length[1]	L_{CA}	60	μm	—
Muscle membrane capacitance[2]	C_m^j	6.5	pF	0, 1, 2
Endothelium compartment capacitance[3,4,5]	C_e^j	0.41	pF	0, 1, 2
Muscle–muscle gap-junctional conductance[3,4,5]	g_{mm}^j	6175	pS	0, 1, 2
Muscle–endothelium gap-junctional conductance[3,4,5]	g_{me}^j	553	pS	0, 1, 2
Endothelium–endothelium gap-junctional conductance[3,4,5]	g_{ee}^j	12350	pS	0, 1, 2
Whole muscle leak conductance[3,4,5,6]	g_{L}^{j}	6.5	pS	0, 1, 2
Whole muscle potassium conductance[3,4,5,6]	g_{K}^{j}	26	pS	0, 1, 2
Whole muscle calcium conductance[3,4,5,6]	g_{Ca}^{j}	13	pS	0, 1, 2
Leak reversal potential[3,4,5,6]	v_{L}^{j}	−70	mV	0, 1, 2
Potassium reversal potential[3,4,5,6]	v_{K}^{j}	−95	mV	0, 1, 2
Calcium reversal potential[3,4,5,6]	v_{Ca}^{j}	80	mV	0, 1, 2
Myogenic response minimum current[3]	$I_{\mathrm{MR,min}}^{j}$	−32	fA	0, 1, 2
Myogenic response maximum current[3]	$I_{\mathrm{MR,max}}^{j}$	195	fA	0, 1, 2
Myogenic response sensitivity[3]	s_{MR}^{j}	0.06	mmHg^{-1}	0, 1, 2
Tubuloglomerular feedback minimum current[3]	$I_{\mathrm{TGF,min}}^{j}$	−80	fA	1, 2
Tubuloglomerular feedback maximum current[3]	$I_{\mathrm{TGF,max}}^{j}$	60	fA	1, 2
Tubuloglomerular feedback sensitivity[3]	s_{TGF}^{j}	0.16	mM^{-1}	1, 2

B2). The oscillating TGF signal in nephron 2 propagates along the two arterioles and drives nephron 1, whose TGF has been inhibited, to oscillate too.

The propagation of the TGF signal is mediated by two pathways: (i) electrotonic conduction along the smooth muscle and endothelium layers of the arteriolar walls, and (ii) blood flow hydrodynamics. Electrotonic conduction (i) induces simultaneous vasoconstriction in both nephrons, whereas, owing to mass conservation, hydrodynamic coupling (ii) induces opposing changes in the two nephrons. Both pathways are represented in Fig. 3(B1 and B2). Synchronicity of the oscillations suggests the dominance of the electrotonic pathway over hydrodynamics. To further clarify the importance of electrotonic conduction, we set g_{mc}^{*} and g_{ec}^{*} to zero, thereby completely disabling pathway (i). The resulting SNGFR and macula densa $[\mathrm{Cl}^{-}]$ are shown in Fig. 3(C1 and C2). The TGF-mediated macula densa $[\mathrm{Cl}^{-}]$ oscillations become out of phrase and significantly weaker relative to those in Fig. 3(B1 and B2).

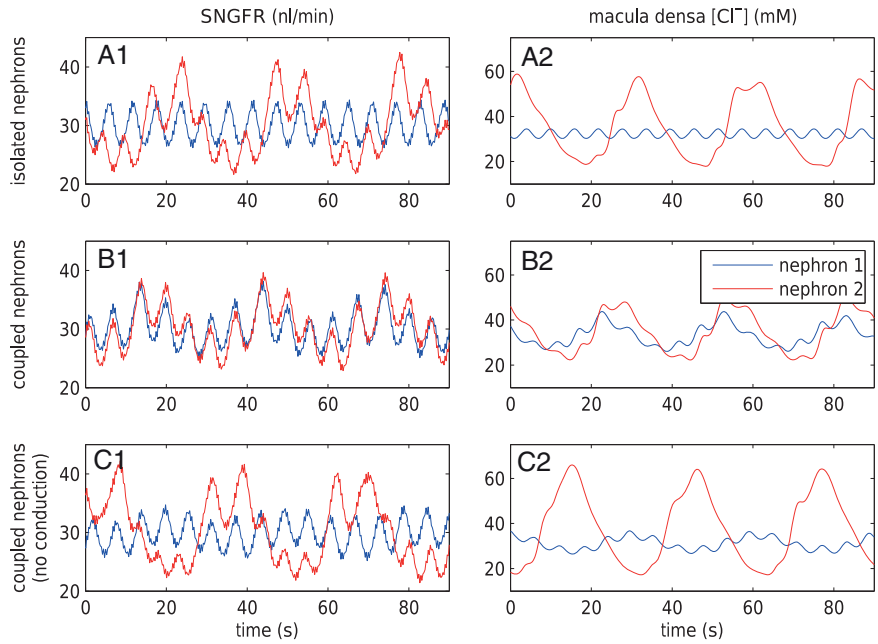

FIG. 3. Effect of internephron coupling on SNGFR and macula densa [Cl^-]. TGF is disabled in nephron 1; TGF gain is set to 3.1 in nephron 2. (A1 and A2) Isolated nephrons. TGF-mediated oscillations are seen in nephron 2. (B1 and B2) Fully coupled nephrons show synchronization of myogenic and TGF-mediated oscillations. (C1 and C2) Electrotonic conduction disabled. Oscillations in nephron 1 are induced by hydrodynamic coupling and are much weaker compared with the fully coupled case (B1 and B2).

3.2 *Estimation of internephron coupling coefficient*

In the next set of simulations, we determine ϕ, which quantifies the ability of one nephron to influence the other nephron's SNGFR via TGF. To that end, we disable TGF in nephron 2 (by fixing C^2_{MD} at 32 mM), vary C^1_{MD} values from 30 to 34 mM, and compute changes in the two nephrons' SNGFR. As previously noted, even in the absence of TGF, tubular flow and other variables exhibit oscillations owing to the spontaneous vasomotion and, to a lesser extent due to heart beat. Thus, to estimate internephron coupling strength, we use time-averaged SNGFR values for each nephron. The predicted SNGFR of both nephrons, as functions of C^1_{MD}, are shown in Fig. 4(A). Owing to the decay of the electrotonic signal along the afferent arterioles, perturbations in $\bar{Q}^2_{\mathrm{F}}$ are smaller than in $\bar{Q}^1_{\mathrm{F}}$. Fig. 4(B) shows the ratio of these perturbations. This ratio provides an estimation of the internephron coupling coefficient ϕ, which is defined as this ratio evaluated at the operating macula densa [Cl^-], i.e.

$$\phi = \left. \frac{\partial \bar{Q}^2_{\mathrm{F}} / \partial C^1_{\mathrm{MD}}}{\partial \bar{Q}^1_{\mathrm{F}} / \partial C^1_{\mathrm{MD}}} \right|_{C^1_{\mathrm{MD}} = \bar{C}^1_{\mathrm{MD}}} . \tag{3.1}$$

The baseline coupling coefficient is $\phi = 0.17$, which is consistent with experimental observation (Chen *et al.*, 1995).

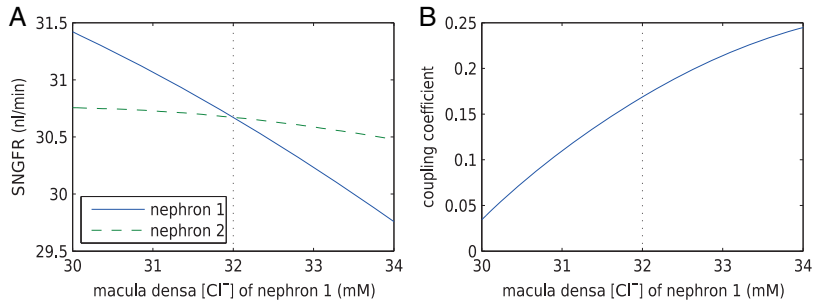

FIG. 4. Open-loop simulations to estimate internephron coupling coefficient. (A) SNGFR for the two nephrons as a function of C^1_{MD}, with C^2_{MD} set to 32 mM. (B) Corresponding coupling coefficient, given by the ratio of the two SNGFR values.

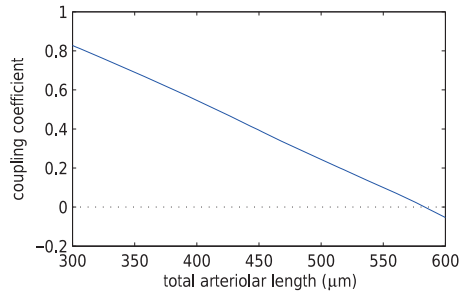

FIG. 5. Internephron coupling coefficient as a function of total arteriolar length. Dependence is approximately linear.

3.2.1 *Effect of afferent arteriole length on internephron coupling.* Because the electrotonic signal decays along the afferent arterioles, ϕ is expected to be a decreasing function of vessel length. Figure 5(A) shows ϕ as a function of total afferent arteriole length (sum of the lengths of the two arterioles). These results were obtained with the assumption that the two model arterioles are of identical length. Anatomic findings have yielded a range of afferent arteriole lengths, $\sim$ 200–500 μm (Casellas *et al.*, 1994; Nordsletten *et al.*, 2006). Given these estimates, our model suggests that ϕ ranges in an approximately linear fashion, from nearly 90% at a total arteriolar length of 300 μm, to nearly 0 at 600 μm. It is interesting that for sufficiently long arterioles, ϕ becomes negative, which indicates a shift in the dominant pathway from electrotonic conduction to hydrodynamics.

3.2.2 *Internephron coupling sensitivity on gap-junctions.* Electrotonic signal propagation between the two nephrons is mediated by gap-junctions developed at the interfaces of smooth muscle and endothelium cells. Each interface is associated with a different conductance, and thus impacts ϕ differently. To assess the impact of these conductances on ϕ, we conducted simulations where we separately varied each conductance by $\pm 20\%$ of its baseline value. Results, which are summarized in Fig. 6, indicate that ϕ is most sensitive to g_{mm} and g_{ee}. In contrast, ϕ appears relatively insensitive to conductances developed near the vascular junction (i.e. g_{mc}, g_{ec}, g^*_{mc}, g^*_{ec}). This suggests that geometric considerations near the vascular junction do not have a significant impact on overall coupling strength.

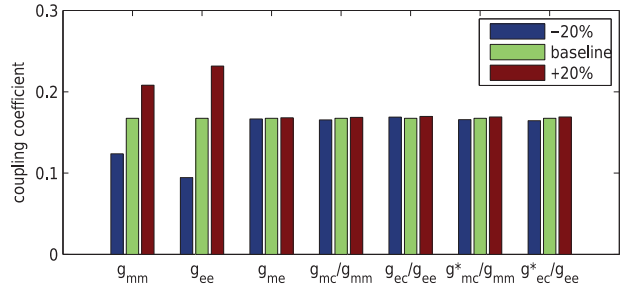

FIG. 6. Percentage changes in coupling coefficient changes as gap-junctional parameters are varied by ±20% from baseline values. Coupling strength is most sensitive to g_{mm} and g_{ee}.

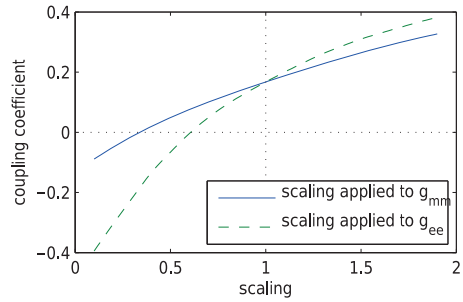

FIG. 7. Internephron coupling coefficient ϕ as a function of scaling applied to either g_{mm} or g_{ee}.

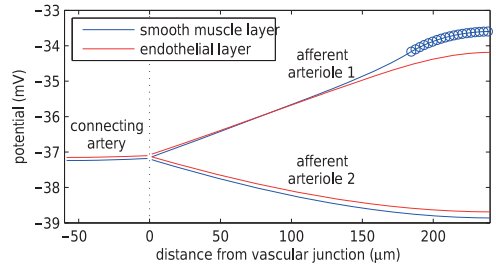

FIG. 8. Time average smooth muscle and endothelium potential profiles under maximal stimulation of TGF at nephron 1. Circles denote the TGF application site. Length constant of depolarization is longer in endothelium than in smooth muscle.

Next we compare the relative contributions of the smooth muscle and endothelial pathways in the conduction of the TGF signal. To that end, we individually vary g_{mm} and g_{ee}, from 10% to about 200% its baseline value, and compute the resulting coupling coefficient ϕ. As can be observed from Fig. 7, the dependence of ϕ on g_{ee} is significantly stronger than that on g_{mm}. This implies the majority of the TGF signal is conducted via the endothelial layer. This is further illustrated in Fig. 8, which shows the membrane potential of the smooth muscle and endothelial cells along the arterioles, as well as the connecting artery, under maximal stimulation of TGF. One can see that the signal decays more rapidly along the smooth muscle layer, owing to its lower gap-junctional conductance, relative to the endothelial layer.

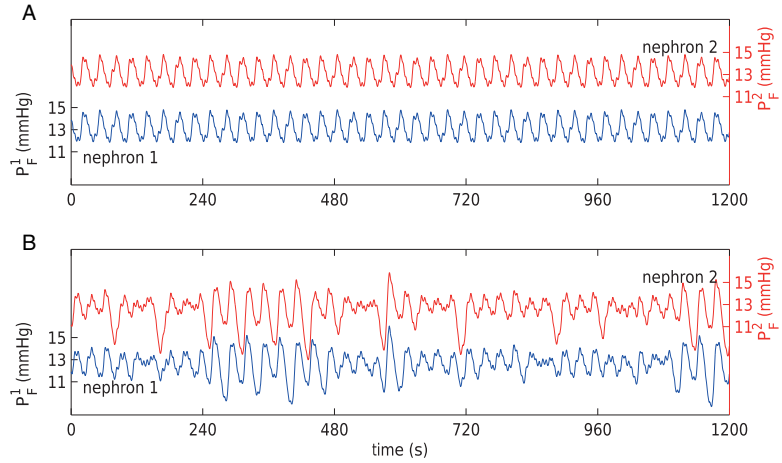

FIG. 9. Proximal tubule pressure oscillations for baseline (A) and reduced (B) gap-junctional conductances. Irregular oscillations are obtained for the lower conductances.

3.3 *Effect of gap-junctions on TGF responses*

As noted above, the baseline model exhibits regular oscillations with key frequencies at ∼170 mHz and ∼30 mHz (Fig. 3), which correspond to oscillations mediated by spontaneous ionic fluxes and TGF, respectively. Those oscillations are transmitted to blood and solute flows through the contractile mechanics of the vascular smooth muscles of the arteriolar walls. Fluctuations in the myogenic tone of a given smooth muscle is initiated by changes in its membrane potential, which is coupled to that of the neighbouring smooth muscles via the gap-junctions.

Gap-junctional coupling is known to be altered in hypertension (Rummery & Hill, 2004; Figueroa *et al.*, 2006; Wagner, 2008; Brisset *et al.*, 2009; Figueroa & Duling, 2009), and blood flow in spontaneously hypertensive rats has been observed to exhibit highly irregular oscillations (Holstein-Rathlou & Marsh, 1994). Thus, we seek to investigate the role of gap-junctional coupling in maintaining or disrupting the regularity of flow oscillations. To that end, we computed the time courses of proximal tubule pressure for a range of gap-junctional conductance values. Two selected cases are shown in Fig. 9: (A) corresponds to baseline g_{mm}, g_{ee}, g_{me}, and (B) to the same parameters reduced by 55% of the baseline values. As can be seen, the lower conductances yield highly irregular oscillations. In none of the simulations with conductances higher than baseline did we observe similarly irregular oscillations (results not shown).

The spontaneously hypertensive rats that exhibit irregular oscillations (Holstein-Rathlou & Marsh, 1994) have also been found to exhibit stronger vasomotor coupling among neighbouring nephrons (Wagner *et al.*, 1997). To better understand the relation between gap-junctional conductance and vasomotor coupling strength, we conducted open TGF-loop simulations for conductances at baseline values and reduced by 55%, as above. In both simulations, C^2_{MD} was kept at 32 mM, and C^1_{MD} was chosen to yield a local vasoconstriction of ∼20%. Figure 10 shows the resulting profiles of time-averaged muscle potential and vasoconstriction along the afferent arterioles. Reduced gap-junctional conductances appear to yield stronger conducted responses in both membrane potential and vasoconstriction.

To understand the above predictions, which may appear counter-intuitive, we revisit the spontaneous limit-cycle oscillations of the smooth muscle membrane potential, which arise from the interactions

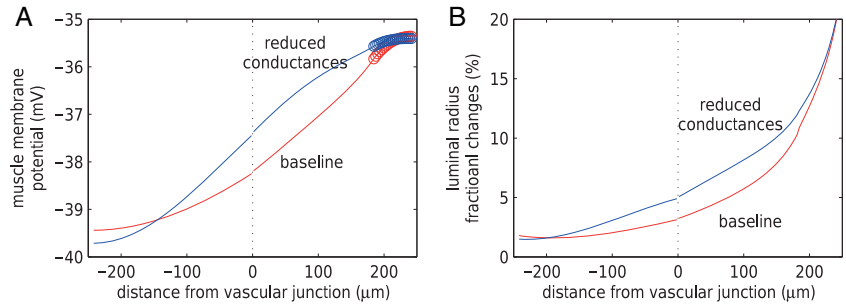

FIG. 10. (A) Time-averaged muscle potential profiles for baseline g_{mm}, g_{ee}, g_{me} values, and for conductances reduced by 55%. Circles denote TGF application sites. Stimulated nephron is shown on the right (positive distance); paired nephron on the left (negative distance). Dotted line indicates the location of the vascular junction. (B) Corresponding vasomotor responses. Reduced conductances yield stronger coupling.

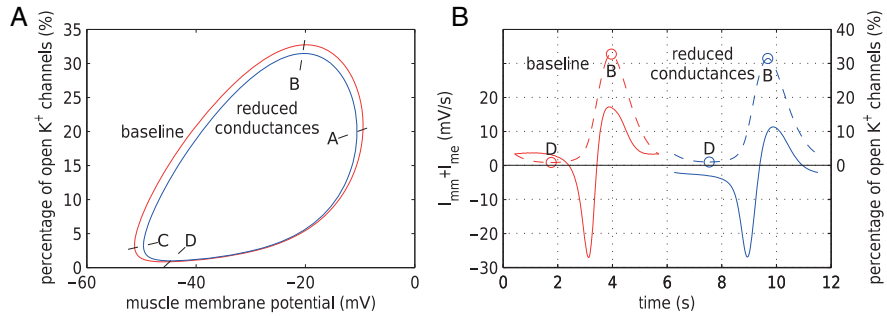

FIG. 11. (A) Limit cycles of muscle potential and K^+ channels opening of afferent arteriole smooth muscle cells located 200 μm upstream of the TGF application site. Trajectories are counterclockwise for both cycles. (B) Time courses of net gap-junctional current $I^{i,j}_{mm} + I^{i,j}_{me}$ (solid lines) and fraction of open K^+ channels (dashed lines).

between the membrane potential, and the voltage-gated Ca^{2+} and K^+ channels (Equations (2.4) and (2.5)). Figure 11(A) shows the limit cycles of the smooth muscle located 200 μm upstream of the TGF application site, for the simulations with baseline and reduced conductances. Each cycle can be divided into four regions, according to the open state of the Ca^{2+} and K^+ channels: A→B, where Ca^+ channels close and K^+ channels open; B→C, where Ca^+ and K^+ channels close; C→D, where Ca^+ channels open and K^+ channels close; D→A, where Ca^+ and K^+ channels open. Clearly, the electrotonic influence is stronger along A→B→C, which is associated with the closing of K^+ channels, than along C→D→A, which is associated with the opening of K^+ channels. Owing to the gap-junctional communications among the smooth muscles, different conductances yield different deformations of the limit cycles. In particular, the reduced conductances case yield a smaller limit cycle. How does this explain the stronger vasoconstriction?

To answer this question, we consider the net gap-junctional currents (between two smooth muscle cells, and between smooth muscle and endothelial cells, $I^{i,j}_{mm} + I^{i,j}_{me}$). As shown in Fig. 11(B), the reduced conductance values yield smaller currents than the base case (compare maximum currents at 11.3 (reduced) versus 17.2 mV/s (baseline), minimum currents at −26.8 (reduced) versus −27.0 mV/s (baseline)). This is to be expected and does not explain the stronger coupling in the reduced conductance

case. However, consider point B, which marks the beginning of the closing of the K^+ channels. Coincidentally, B is close to the peaks of $I^{i,j}_{mm} + I^{i,j}_{me}$ in both cases. That current is depolarizing, which opposes the closing of the K^+ channels. Thus, the stronger the current, the slower is the closing of K^+ channels. Because $I^{i,j}_{mm} + I^{i,j}_{me}$ is stronger with the baseline conductances, K^+ channels are prone to slower closing. To quantify these observations, we compute the time-averaged fraction of open K^+ channels $\bar{n}^{i,j}$ by

$$\bar{n}^{i,j} = \frac{\bar{I}^{i,j}_{\mathrm{K}}}{g^{i,j}_{\mathrm{K}}(\bar{v}^{i,j}_m - v^{i,j}_{\mathrm{K}})}, \tag{3.2}$$

where $\bar{v}^{i,j}_m$ and $\bar{I}^{i,j}_{\mathrm{K}}$ are the corresponding time averages of $v^{i,j}_m$ and $I^{i,j}_{\mathrm{K}}$. For the muscles shown in Fig. 11, $\bar{n}^{i,j} = 12.6\%$ and 11.2% for baseline and reduced conductances, respectively. Consequently, the time-averaged membrane potentials are $\bar{v}^{i,j}_m = -38.1$ and -36.2 mV, respectively. That is, the reduced conductances result in a larger degree of depolarization, and a stronger vasoconstrictive response (radius 9.3 μm compared with 9.6 μm in the base case).

4. Discussion

We have extended our previous detailed model of renal haemodynamics (Sgouralis & Layton, 2014b) to represent two coupled nephrons. The resulting coupled nephron model is used to study electrotonic conduction of TGF signal between coupled nephrons, factors that impact the coupling strength, and the effect of internephron coupling on TGF-mediated dynamics.

4.1 *Comparison with previous modelling studies*

In a series of studies (Layton *et al.*, 2009, 2011; Ryu & Layton, 2014), we have previously used mathematical models to investigate the effects of internephron coupling on TGF-mediated dynamics. A major difference between the present study and the previous studies is that the latter represent only electrical coupling, whereas by including the afferent arterioles and connecting artery, the present study represents both hydrodynamic and electrical coupling.

Another major difference is that the previous models (Layton *et al.*, 2009, 2011; Ryu & Layton, 2014) do not explicitly incorporate the afferent arterioles. Instead, internephron coupling is represented by applying a fraction (determined by a coupling parameter, ϕ) of the TGF signal of the initiating nephron to its paired nephron. This implies that the coupling strength is known *a priori*. In contrast, the present model explicitly represents two paired afferent arterioles, along which the TGF signal propagates. This allows us to determine the internephron coupling strength. The base case coupling strength, $\phi = 0.17$, agrees well with values assumed in our previous studies (Layton *et al.*, 2009, 2011; Ryu & Layton, 2014).

In a pioneering study, Marsh *et al.* (2013) published a similarly comprehensive model of a nephrovascular network that incorporates a large number of afferent arterioles, loops of Henle and TGF. In that model, each afferent arteriole is represented by only two myogenically active segments. Thus, each submodel represents a rather long segment along the afferent arteriole, whereas in the present study, each afferent arteriolar cell submodel has the dimensions of a renal smooth muscle cell (Loutzenhiser & Loutzenhiser, 2000). Also, the model of Marsh *et al.* (2013) uses a phenomenological representation of TGF signal propagation; the TGF input is applied to both arteriolar segments with a predefined decay based on the distance from the glomerulus. In contrast, in the current model TGF input is applied only to

the distal smooth muscles of each arteriole and the signal propagates along the arterioles via electronic conduction.

4.2 *Internephron coupling and hypertension*

In the cardiovascular system, gap-junctions are made up of one or more of four connexin proteins: Cx37, Cx40, Cx43 and Cx45. Changes in Cx expression in hypertensive animal models have been reported, although those results are not always consistent. Cx40 and Cx45 are consistently reduced in endothelial cells, but results for Cx43 are mixed (Haefliger *et al.*, 2000; Yeh *et al.*, 2006). An interesting and likely relevant observation is that normalization of blood pressure in the spontaneously hypertensive rats using an angiotensin-converting enzyme inhibitor or candesartan restores endothelial connexin expression to normal in parallel with the normalization of blood pressure (Kansui *et al.*, 2004; Rummery *et al.*, 2005).

Our simulation results suggest that a reduction in gap-junctional conductances elevates internephron coupling, in the sense that it yields a stronger conducted TGF response (Fig. 11). This rather surprising prediction is a result of the interactions between the gap-junctional voltage signal and the K^+ channels. Assuming that gap-junctional conductances are indeed reduced in spontaneously hypertensive rats, our result may explain the observed stronger TGF coupling (Wagner *et al.*, 1997). There is experimental evidence which suggests that gap-junctional conductances may vary in different disease states (Heberlein *et al.*, 2009). The relation between gap-junctional conductances and TGF coupling strength predicted by the present model can be tested provided these quantities can be measured in health and disease states.

Additionally, our simulation results suggest that reduced conductances give rise to irregular TGF-mediated oscillations in nephron flows and related variables (Fig. 9). Similar patterns have been observed in spontaneously hypertensive rats (Holstein-Rathlou & Marsh, 1994). This prediction is also consistent with findings by de Wit *et al.* (2003), which indicate that the absence of vascular Cx40 is associated with hypertension and irregular vasomotion. In particular, de Wit *et al.* reported diameter fluctuations reaching as low as $\sim 0\,\mu$m in $Cx40^{-/-}$ arterioles. Similarly, our model predicts fluctuations reaching near complete occlusion when gap-junctional conductances are reduced to $<40\%$ of baseline values (results not shown).

Note, however, that we have limited our consideration to the effects of altered gap-junctional conductances. Other differences between hypertensive and normotensive animals, e.g. perfusion pressure, TGF gain (Dilley & Arendshorst, 1984), pressure natriuretic and diuretic responses (Granger *et al.*, 2002; Beard & Mescam, 2012), etc. have not been incorporated. These factors will be considered in a future, more comprehensive study that focuses on autoregulation in a hypertensive kidney.

4.3 *Myoendothelial gap-junction expression*

The proper conduction of vasomotor responses relies on a high density of myoendothelial gap-junctions, which provide electrical communication between endothelial cells and smooth muscle cells. The expression of myoendothelial gap-junctions have been reported to be heterogeneous, among different vascular beds, with density inversely related to arteriolar size (Sandow *et al.*, 2012). In a modelling study, Hald *et al.* (2014) show that heterogeneous distributions of myoendothelial gap-junction properties may have a profound impact on system behaviour. However, spatial heterogeneity in myoendothelial gap-junction expression within a given afferent arteriole has yet to be demonstrated, and direct measurements of myoendothelial gap-junction conductances do not exist. Given these uncertainties, we have assumed constant gap-junction conductances in the present model. Nonetheless, the impact of heterogeneous myoendothelial gap-junction distributions is a worthwhile consideration in a future study.

Funding

This research was supported by the National Institutes of Health: National Institute of Diabetes and Digestive and Kidney Diseases, Grant DK089066. Part of the work was conducted while I.S. was a Postdoctoral Fellow at the National Institute for Mathematical and Biological Synthesis, an Institute sponsored by the National Science Foundation through NSF Award #DBI-1300426, with additional support from The University of Tennessee, Knoxville.

References

Beard, D. & Mescam, M. (2012) Mechanisms of pressure-diuresis and pressure-natriuresis in Dahl salt-resistant and Dahl salt-sensitive rats. *BMC Physiol.*, **12**, 6.

Brink, P. (1998) Gap junctions in vascular smooth muscle. *Acta Physiol. Scand.*, **164**, 349–56.

Brisset, A., Isakson, B. & Kwak, B. (2009) Connexins in vascular physiology and pathology. *Antioxid Redox Signal*, **11**, 267–282.

Casellas, D., Dupont, M., Bouriquet, N., Moore, L., Artuso, A. & Mimran, A. (1994) Anatomic pairing of afferent arterioles and renin cell distribution in rat kidneys. *Am. J. Physiol.*, **267**, F931–F936.

Chen, J., Sgouralis, I., Moore, L., Layton, H. & Layton, A. (2011) A mathematical model of the myogenic response to systolic pressure in the afferent arteriole. *Am. J. Physiol. Renal Physiol.*, **300**, F669–F681.

Chen, Y., Yip, K., Marsh, D. & Rathlou, N. H. (1995) Magnitude of TGF-initiated nephron-nephron interaction is increased in SHR. *Am. J. Physiol.*, **269**, F198–F204.

Chilton, L., Loutzenhiser, K., Morales, E., Breaks, J., Kargacin, G. & Loutzenhiser, R. (2008) Inward rectifier k(+) currents and kir2.1 expression in renal afferent and efferent arterioles. *J. Am. Soc. Nephrol.*, **19**, 69–76.

Christensen, J. & Bohle, A. (1978) The juxtaglomerular apparatus in the normal rat kidney. *Virchows Arch. A Path Anat. and Histol.*, **379**, 143–150.

de Wit, C., Roos, F., Bolz, S.-S., and Pohl, U. (2003) Lack of vascular connexin 40 is associated with hypertension and irregular arteriolar vasomotion. *Physiol. Genom.*, **13**, 169–177.

Dilley, J. & Arendshorst, W. (1984) Enhanced tubuloglomerular feedback activity in rats developing spontaneous hypertension. *Am. J. Physiol.*, **247**, F672–F679.

Eaton, D. & Pooler, J. (2004) *Vander's Renal Physiology*, 6th edn. New York: McGraw-Hill Medical.

Figueroa, X. & Duling, B. (2009) Gap junctions in the control of vascular function. *Antioxid Redox Signal*, **11**, 251–266.

Figueroa, X., Isakson, B. & Duling, B. (2006) Vascular gap junctions in hypertension. *Hypertension*, **48**, 804–811.

Granger, J., Alexander, B. & Llinas, M. (2002) Mechanisms of pressure natriuresis. *Curr. Hypertens Rep.*, **4**, 152–159.

Haefliger, J., Polikar, R., Schnyder, G., Burdet, M., Sutter, E., Pexieder, T., Nicod, P. & Meda, P. (2000) Connexin37 in normal and pathological development of mouse heart and great arteries. *Dev. Dyn.*, **218**, 331–344.

Hald, B., Jacobsen, J., Sandow, S., Holstein-Rathlou, N.-H. & Welsh, D. (2014) Less is more: minimal expression of myoendothelial gap junctions optimizes cell-cell communication in virtual arterioles. *J. Physiol.*, **15**, 3243–3255.

Han, J., Thompson, K., Chou, C. & Knepper, M. (1992) Experimental tests of three-dimensional model of urinary concentrating mechanism. *J. Am. Soc. Nephrol.*, **2**, 1677–1688.

Heberlein, K., Straub, A. & Isakson, B. (2009) The myoendothelial junction: breaking through the matrix? *Microcirculation*, **16**, 307–322.

Holstein-Rathlou, N. (1987) Synchronization of proximal intratubular pressure oscillations: evidence for interaction between nephrons. *Pflügers Arch.*, **408**, 438–443.

HOLSTEIN-RATHLOU, N. & MARSH, D. (1994) Renal blood flow regulation and arterial pressure fluctuations: a case study in nonlinear dynamics. *Physiol. Rev.*, **74**, 637–681.

JUST, A. (2007) Mechanisms of renal blood flow autoregulation: dynamics and contributions. *Am. J. Physiol. Regul. Integr. Comp. Physiol.*, **292**, R1–R17.

KÄLLSKOG, Ö. & MARSH, D. (1990) TGF-initiated vascular interactions between adjacent nephrons in the rat kidney. *Am. J. Physiol.*, **259**, F60–F64.

KANSUI, Y., FUJII, K., NAKAMURA, K., GOTO, K., ONIKI, H., ABE, I., SHIBATA, Y. & IIDA, M. (2004) Angiotensin II receptor blockade corrects altered expression of gap junctions in vascular endothelial cells from hypertensive rats. *Am. J. Physiol. Heart Circ. Physiol.*, **287**, H216–H224.

LAYTON, A., BOWEN, M., WEN, A. & LAYTON, H. (2011) Feedback-mediated dynamics in a model of coupled nephrons with compliant thick ascending limbs. *Math. Biosci.*, **230**, 115–127.

LAYTON, A., MOORE, L. & LAYTON, H. (2006) Multistability in tubuloglomerular feedback and spectral complexity in spontaneously hypertensive rats. *Am. J. Physiol. Renal Physiol.*, **291**, F79–F97.

LAYTON, A., MOORE, L. & LAYTON, H. (2009) Multistable dynamics mediated by tubuloglomerular feedback in a model of coupled nephrons. *Bull. Math. Biol.*, **71**, 515–555.

LAYTON, H., PITMAN, E. & MOORE, L. (1991) Bifurcation analysis of TGF-mediated oscillations in SNGFR. *Am. J. Physiol.*, **261**, F904–F919.

LOUTZENHISER, R., BIDANI, A. & CHILTON, L. (2002) Renal myogenic response: kinetic attributes and physiologic role. *Circ. Res.*, **90**, 1316–1324.

LOUTZENHISER, R., BIDANI, A. & WANG, X. (2004) Systolic pressure and the myogenic response of the renal afferent arteriole. *Acta Physiol. Scand.*, **181**, 404–413.

LOUTZENHISER, K. & LOUTZENHISER, R. (2000) Angiotensin ii-induced ca(2+) influx in renal afferent and efferent arterioles: differing roles of voltage-gated and store-operated ca(2+) entry. *Circ. Res.*, **87**, 551–557.

MARSH, D., WEXLER, A., BRAZHE, A., POSTNOV, D., SOSNOVTSEVA, O. & RATHLOU, N. H. (2013) Multinephron dynamics on the renal vascular network. *Am. J. Physiol. Renal Physiol.*, **304**, F88–F102.

NORDSLETTEN, D., BLACKETT, S., BENTLEY, M., RITMAN, E. & SMITH, N. (2006) Structural morphology of renal vasculature. *Am. J. Physiol. Heart Circ. Physiol.*, **291**, H296–H309.

NYENGAARD, J. & BENDTSEN, T. (1992) Glomerular number and size in relation to age, kidney weight, and body surface in normal man. *Anat. Rec.*, **232**, 194–201.

PITMAN, E., ZARITSKI, R., KESSELER, K., MOORE, L. & LAYTON, H. (2004) Feedback-mediated dynamics in two coupled nephrons. *Bull. Math. Biol.*, **66**, 1463–1492.

RUMMERY, N., GRAYSON, T. & HILL, C. (2005) Angiotensin-converting enzyme inhibition restores endothelial but not medial connexin expression in hypertensive rats. *J. Hypertens.*, **23**, 317–328.

RUMMERY, N. & HILL, C. (2004) Vascular gap junctions and implications for hypertension. *Clin. Exp. Pharmacol. Physiol.*, **31**, 659–667.

RYU, H. & LAYTON, A. (2014) Tubular fluid flow and distal NaCl delivery mediated by tubuloglomerular feedback in the rat kidney. *J. Math. Biol.*, **68**, 1023–1049.

SANDOW, S., SENADHEERA, S., BERTRAND, P., MURPHY, T. & TARE, M. (2012) Myoendothelial contacts, gap junctions, and microdomains: anatomical links to function? *Microcirculation*, **19**, 403–415.

SGOURALIS, I. & LAYTON, A. (2012) Autoregulation and conduction of vasomotor responses in a mathematical model of the rat afferent arteriole. *Am. J. Physiol. Renal Physiol.*, **33**, F229–F239.

SGOURALIS, I. & LAYTON, A. (2014a) Control and modulation of fluid flow in the rat kidney. *Bull. Math. Biol.*, **306**, F1357–F1371.

SGOURALIS, I. & LAYTON, A. (2014b) Theoretical assessment of renal autoregulatory mechanisms. *Am. J. Physiol. Renal Physiol.*, **306**, F1357–F1371.

THOMSON, S. & BLANTZ, R. (2008) Glomerulotubular balance, tubuloglomerular feedback, and salt homeostasis. *J. Am. Soc. Nephrol.*, **19**, 2272–2275.

THOMSON, S., DENG, A., BAO, D., SATRIANO, J., BLANTZ, R. & VALLON, V. (2001) Ornithine decarboxylase, kidney size, and the tubular hypothesis of glomerular hyperfiltration in experimental diabetes. *J. Clin. Invest.*, **107**, 217–224.

Wagner, C. (2008) Function of connexins in the renal circulation. *Kidney Int.*, **73**, 547–555.
Wagner, A., Holstein-Rathou, N. & Marsh, D. (1997) Internephron coupling by conducted vasomotor responses in normotensive and spontaneously hypertensive rats. *Am. J. Physiol.*, **272**, F372–F379.
Yeh, H., Lee, P., Su, C., Tian, T., Ko, Y. & Tsai, C. (2006) Reduced expression of endothelial connexins 43 and 37 in hypertensive rats is rectified after 7-day carvedilol treatment. *Am. J. Hypertens.*, **19**, 129–135.
Yip, K., Holstein-Rathlou, N. & Marsh, D. (1992) Dynamics of TGF-initiated nephron-nephron interactions in normotensive rats and SHR. *Am. J. Physiol.*, **262**, F980–F988.